

# OPTICAL NAVIGATION FOR THE DAWN MISSION AT VESTA

Nickolaos Mastrodemos<sup>(1)</sup>, Brian Rush<sup>(2)</sup>, Drew Vaughan<sup>(3)</sup>, William Owen Jr.<sup>(4)</sup>

<sup>(1)(2)(3)(4)</sup> *Optical Navigation Group, Mission Design and Navigation Section,  
Jet Propulsion Laboratory, California Institute of Technology,  
Pasadena, CA, 91109*

<sup>(1)</sup> MS 264-820, (818) 393-2477, [mastrode@jpl.nasa.gov](mailto:mastrode@jpl.nasa.gov)

<sup>(2)</sup> MS 264-820, (818) 458-1998, [Brian.P.Rush@jpl.nasa.gov](mailto:Brian.P.Rush@jpl.nasa.gov)

<sup>(3)</sup> MS 264-820, (818) 393-5141, [Andrew.T.Vaughan@jpl.nasa.gov](mailto:Andrew.T.Vaughan@jpl.nasa.gov)

<sup>(4)</sup> MS 301-121, (818) 354-2505, [wmo@jpl.nasa.gov](mailto:wmo@jpl.nasa.gov)

**Abstract:** *The Dawn S/C was launched in September 2007 in order to perform remote sensing observations of the asteroids Vesta and Ceres. Dawn entered into orbit about Vesta in July 2011, completed successfully the mission goals, that were carried out in four different science orbits, by August 2012 and has since departed towards asteroid Ceres. An important component of the Dawn navigation was optical navigation, which was performed at almost all mission phases. Optical data types were used in the overall orbit determination process. In addition they were used to determine some key aspects of the asteroid's physical characteristics, such as the rotational axis, shape and surface morphology and gravity terms. In this paper we present an overview of the optical navigation operations at Vesta, the optical navigation planning, image acquisition strategy, data reduction methodology, and the up-to-date post operations assessment. Of particular importance is the extensive use of landmark navigation, which was performed for the first time for real-time support of operations and which comprised the bulk of the optical data processing.*

**Keywords:** *optical navigation, orbital operations, image processing, landmark.*

## 1. Introduction

The Dawn S/C was launched in September 2007 towards asteroids Vesta and Ceres[1], in order to conduct remote sensing observations of their surface, interior and elemental composition. The payload consists of two optical instruments, or Framing Cameras 1 & 2 (FC1, FC2), a Visual and Infrared Mapping Spectrometer (VIR) and a gamma ray and neutron detector (GRaND). In addition radiometric data are collected to determine the gravity field, [2],[3],[4],[5], [6],[7]. Dawn is a low-thrust mission [8],[9]; most of the impulse needed to reach its destinations is provided by one of its three ion-propulsion engines, which run almost continuously during the ~3 ½ of the cruise phase. In addition, the maneuvers designed during cruise and orbital operations were also conducted with one of the ion-propulsion engines[10],[11],[12],[13],[14]. Dawn began its approach operations phase towards Vesta on May 2 2011 and was captured by Vesta on July 14 2011. Subsequently it transferred to 4 science orbits, each with distinct orbital characteristics, scientific goals and duration; Survey, High Altitude Mapping Orbit 1 (HAMO-1) Low Altitude Mapping Orbit (LAMO) and HAMO-2. Following the successful completion of the last science orbit Dawn has spiraled out and escaped Vesta on Sep 5 2012. During the science orbits Dawn would strictly coast, acquiring and downlinking science data, with the

exception of LAMO where five Orbital Maintenance Maneuvers (OMM) were performed for safety reasons, namely to avoid Dawn going into eclipse. During approach and transfers Dawn would mostly be in continuous thrusting with the exception of a few coasting opportunities for collecting radiometric and optical data and for engineering telemetry.

An important component of the Orbit Determination process is optical navigation (OpNav), which was used at all mission phases with the exception of the transfer from LAMO to HAMO-2. Optical data are complementary to the traditional radiometric range and Doppler data and often allow visibility in directions perpendicular to the radiometric data. Optical navigation was used to support real-time operations, to determine some key physical characteristics of Vesta, such as the asteroid's pole, shape and gravity terms and to support trajectory reconstruction for science applications.

In this work we present a summary of the OpNav Dawn operations, which includes a summary of the mission phases, Dawn cameras and their calibration, OpNav planning and acquisition, data types and data reduction, and in-flight performance. Of particular interest is the application of landmark navigation, which was used extensively during orbital operations. Many details of the in-flight calibrations, image planning, data processing & methodology were presented in [15], to which we refer for more discussion, and for completeness we summarize here.

## 2. Mission phases

The guiding principle of the Vesta science orbits design was that during each one a particular instrument would be prime, collecting the bulk of its data, whereas the other instruments would either ride along or collect data as permitted. This principle determined the types of orbits as well as the payload pointing. Another consideration for the overall design of the mission phases was the solar illumination of Vesta. The rotational axis of Vesta is such that during capture and the beginning of the science investigation, ~ August 2012, the solar latitude was in the southern hemisphere at  $26^\circ$  S resulting in areas northern than  $\sim 50^\circ$  N being dark. In order to image most of the northern latitudes, certain mission phases had to be repeated at a later time, closer to Vesta's equinox. A breakdown of the Vesta operations into the mission phases with a summary of the key scientific investigations is as follows [16];

**Approach phase:** This was mostly a navigation phase that began 100 days prior to orbit insertion. During this phase the range to Vesta decreased from 160,000 km to 3000 km, Dawn was gravitationally captured and then slowly spiraled into orbit. It included many coasting events for radiometric and 24 OpNav acquisition opportunities. Of particular importance are the Rotational Characterization imaging events (RC) during which Vesta is observed over a full rotation period, 5 h 20 min. There are 4 such opportunities, RC1 at 10 km/pixel FC resolution, RC2 at 5 km/pixel and RC3 and its backup RC3b at 0.5 km/pixel. The main scientific investigations are the determination of Vesta's pole direction, phase function and a search for satellites of Vesta.

**Survey:** A circular polar orbit with targeted mean radius 3000 km, and a targeted beta angle, defined as the angle between the orbit plane and the Sun, at  $12^\circ$ - $15^\circ$ . The prime instrument is VIR for the surface spectral and mineral composition. In addition, OpNav images and a number of FC observations of opportunity were acquired. It consists of seven complete orbits, the first six for data collection, and the last as an additional margin time needed for the navigation team

to prepare for the orbit transfer. The choice for the small beta angle is in order to minimize the emission angle, reduce the surface shadowing and therefore allow as large a signal to noise as possible for VIR.

**HAMO-1:** A circular polar orbit with a 900 km mean radius and a targeted beta angle of  $30^\circ$ . It lasts 62 orbits or  $\sim 29$  days and the primary objective is the surface topography from FC images. It is broken into six cycles, where each cycle maps completely once the illuminated surface. During the time period of this phase the Vesta solar latitude is in the south and such that Vesta is illuminated over a latitude range from  $90^\circ$  S to  $\sim 45^\circ$  N. Each cycle has a particular pointing direction with cycles 1 and 6 pointed nadir and the others are fixed non-nadir. In addition a number of VIR frames are acquired.

**LAMO:** polar orbit at a 450 km radius and a targeted beta angle of  $45^\circ$ . This phase was extended to last almost 5 months, and it was primarily devoted to GRaND and gravity science with additional FC and VIR nadir observations as permitted by the downlink bandwidth.

**HAMO-2:** This is a repeat of the 6-cycle HAMO-1 at similar orbital characteristics except that the beta angle at the beginning of this phase was set to  $34^\circ$  and was allowed to slowly drift towards  $27^\circ$  at the end of this phase in order to allow better illumination of the north latitudes. The objective of repeating these observations was to image sufficiently the latitudes between  $50^\circ$  and  $80^\circ$  which were not visible in HAMO-1 so as to allow the topographic reconstruction of Vesta in these areas.

**Departure RC4:** Following departure from HAMO-2 a last rotational characterization set was acquired on August 26<sup>th</sup> at a range of 6000 km in order to image the remaining, as yet unseen north terrain.

Since the science orbits do not include scheduled OMM, except for LAMO, the correct timing and pointing of the science acquisition plan was maintained by adjusting the epoch of the sequences on-board, as well as updating the Dawn-Vesta relative ephemeris on-board so that the Attitude Control System (ACS) could correctly point the payload either towards Vesta nadir or at an offset to the center of Vesta.

### 3. Dawn Cameras

For redundancy, Dawn is equipped with two framing cameras, FC1, and FC2, which are nominally identical and serve image acquisition for both Science and OpNav [3]. The cameras have a 19 mm aperture size, an IFOV of  $93.3 \mu\text{rad}$  and use refractive optics. Light is focused on a standard  $1024 \times 1024$  frame transfer CCD. Both cameras underwent extensive in-flight calibrations. Photometric calibrations imaged Vega and various solar analogs. Geometric calibrations used cluster observations to estimate the focal length, as well as a 5-parameter distortion model. The calibration results allow an astrometric accuracy of  $0.09 - 0.11$  pixels ( $1-\sigma$ ) when imaging a few stars at a minimum signal-to-noise (SNR)  $> 10$ . Cluster observations were also used to estimate the cameras' alignment in the body frame, by comparing inertial pointing established from the camera star measurements to the cameras' pointing from attitude telemetry from ACS. Following the removal of a fixed bias between the two coordinate systems, the

residuals pointing error is  $\sim 1$  FC pixel and is mostly random. The removal of fixed camera misalignments is essential because when in orbit about Vesta it is not possible to image stars and therefore the pointing information from ACS is the only one available. The only important measurement that we were not able to perform prior to the beginning of approach operations were the in-filed and out-of-field stray-light properties in the presence of a very bright object, and hence the effects of the presence of Vesta on adjacent star images was not known until actual operations.

#### **4. Optical data processing**

Optical navigation was used in all mission phases with the exception of the transfer from LAMO to HAMO-2. The main tasks for OpNav were support in the on-going orbit determination and orbit prediction efforts for future maneuver designs and science sequence updates, such as epoch shifts and on-board ephemeris updates, in the science orbit reconstruction, in the Vesta parameter estimation, such as rotational parameters and gravity terms and in the science planning support by providing updates to the Vesta global topography. The key OpNav interfaces were with the sequencing team, for image acquisition sequencing, with the FC team, for image retrieval and with the mission design team for planning purposes and with the orbit determination team for the ongoing exchange of optical observations and updated trajectories.

##### **4.1 Data types**

At the beginning of approach Vesta was already  $\sim 5$  FC pixels across, so the data types used were those of an extended body, limb scans and landmarks. Limb scans were used from the beginning up to late approach (OpNav18), where Vesta was  $>500$  FC pixels. Landmarks were used from mid-approach (RC1) where Vesta was 60 FC pixels across to the end of the mission. During the time period RC1- OpNav18 where both data types were used, a) the limb scans were processed first as an initial step in order to assist in an updated Dawn-Vesta state estimation and b) improved ephemerides for Vesta & Dawn were used as inputs in order to construct landmarks or reprocess existing ones.

Limbs scans are observations of the location of the limb of the object in order to estimate its center of figure (CoF). Scan lines are constructed, usually normal to the predicted limb, which is computed from the projection of an *a-priori* shape model, expressed in spherical harmonics. The *a-priori* shape is either a triaxial ellipsoid or a more arbitrary shape. Both of these options were used. Next a model brightness profile is constructed with an assumed reflectance function, and it is correlated with the brightness profile from the image in order to determine the best limb location and the CoF. The number of scan lines is determined automatically and increases with the size of the body. The accuracy of the method flattens out as the body size increase to  $> \sim 100$  pixels, to  $\sim 1$ -2% of the radius. The inputs to the orbit determination are the pixel, line location of the CoF and if stars have been imaged, an updated camera inertial pointing.

##### **4.2 Landmark processing**

Landmarks are body-fixed vectors from the body center to its surface. A landmark is defined as the center of small digital terrain and albedo model, or landmark map that extends over a fraction

of the surface. Landmarks are not associated with specific surface features and do not depend on the existence of such body features; they require only a modest brightness surface contrast,  $\sim 3-4$ , for the construction of the maps, which are built with stereo-photoclinometry (SPC) [17],[18],[19]. The key steps in constructing landmarks at Vesta were as follows;

1) Approximate locations for the center of maps on the surface are specified mostly based on latitude, longitude. A map pixel scale and grid size is also selected, usually 99x99 pixels. The map scale is chosen in advance based on mission phase and image resolution considerations. A local coordinate system is also constructed with each map, as shown in figure 1. The latitude, longitude coverage of the given image set is known in advance, by running off-line utility surface coverage tools and a tiling scheme is already in place for determining the separation of the map centers.

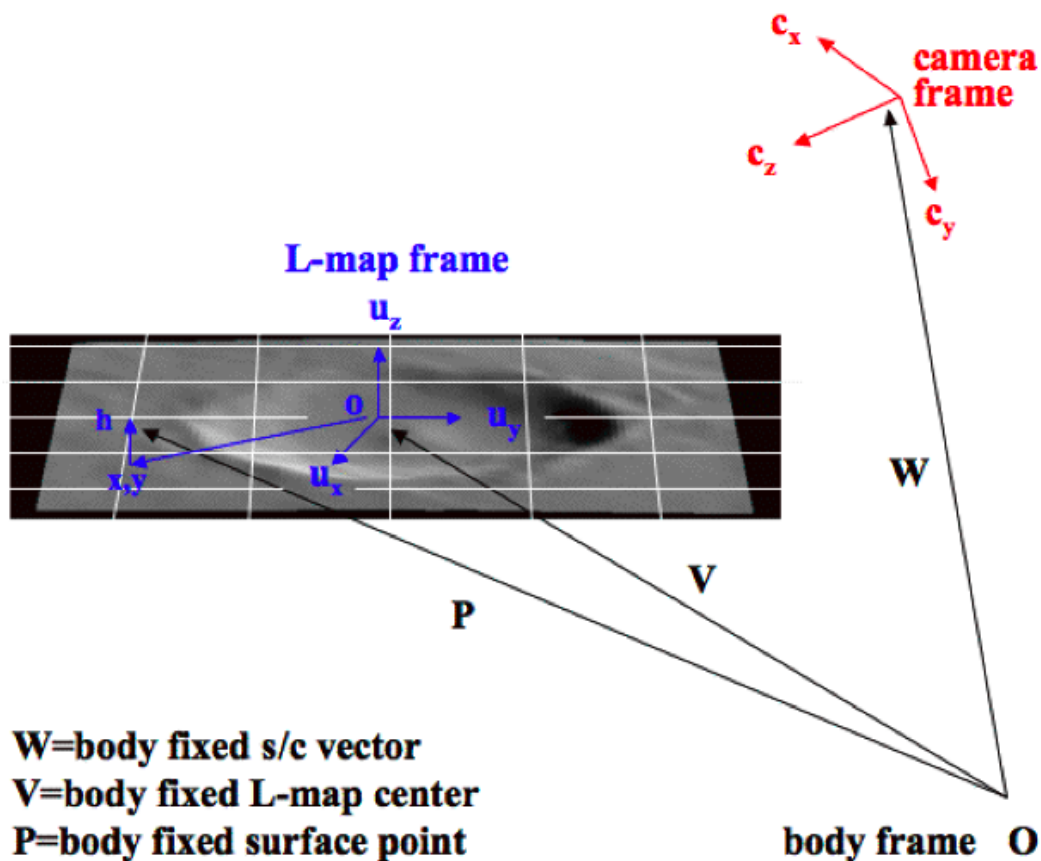


Figure 1. Landmark map geometry

2) Starting with the *a-priori* camera pointing, Dawn & Vesta ephemerides and existing *a-priori* topography or a shape model, all images that could overlap with the map are searched and those that meet certain criteria are retained for the map construction. Such criteria include the range of emission angles, with typical values from  $0^\circ-60^\circ$ , the resolution ratio between map pixel and image pixel, which is usually in the range  $x3 - 1/3$  and the fraction of the illuminated portion of the image that overlaps that of the map, usually  $> 25\%$ . There is no upper limit to the number of images that can be used, however there is a minimum of 3 images needed.

3) For those images that meet the above criteria, the parts that overlap on the newly defined map are extracted, resampled to the map pixel scale and normally projected on the map. Depending on the map resolution the normal to the surface is determined from either an existing *a-priori* shape model or from other coarser maps at resolution higher than the shape model. Because all images are resampled to the map scale images that differ in resolution by a factor as large as 10 or more can be used in the same map. This is particularly the case on approach where the Vesta image resolution varies rapidly.

4) At each pixel  $\mathbf{x}$  of each projected image template that is not dark, a predicted brightness model is constructed,

$$I_k(\mathbf{x}) = \Lambda_k(1+a(\mathbf{x})) R(i,e) + \Phi_k, \quad (1)$$

Where  $a(\mathbf{x})$  is a relative albedo parameter, normalized to have a zero mean over each map,  $k$  is the image index,  $R(i,e)$  is the reflectance function,  $i$  and  $e$  the incidence and emission angles,  $\Lambda_k$  a scale factor and  $\Phi_k$  a background brightness value. The photometric model connects the local slopes in each map pixel,  $(t_1,t_2)$ , along the two horizontal map directions to the imaging geometry via,

$$\cos(i) = (s_3-s_1t_1-s_2t_2)/\sqrt{(1+t_1^2+t_2^2)}, \quad \cos(e) = (c_3-c_1t_1-c_2t_2)/\sqrt{(1+t_1^2+t_2^2)} \quad (2)$$

where  $\mathbf{c}$  is the camera unit vector and  $\mathbf{s}$  the body-sun unit vector. The reflectance function in its simplest form is a linear combination of Lambert and Lommel-Seeliger laws but it can include phase angle terms as well. For most of orbital operations, the spatial extend of each map is small enough that there is very small phase variation so the lack of a detailed phase function is not considered a limitation.

5) At each map pixel the slopes and albedo are estimated by minimizing via weighted least squares the difference between the extracted image brightness template and the model image brightness of equation (1), while also solving for the per-image scale factor and background values,  $\Lambda_k$  and  $\Phi_k$ . During the first step of this stage, due to random pointing errors from image to image and also due to larger projection errors for images at large off-nadir angles, the mean brightness model is often fuzzy. The next step is to re-illuminate the brightness model at the geometry of each individual image, and cross correlate each image template with the average brightness model. An image shift is computed from the peak of the correlation measure and applied to every image. The process is repeated starting with step 4 above until the shifts become very small, typically  $< 0.01$  map pixels. Images that for various reasons, e.g., too dark or with large projection errors, show poor correlation may be discarded at this stage and re-introduced later. This process also modifies the pixel, line location of the landmark in each image, and therefore the observations. Figure 2 shows the endpoint of such a process from late approach. The first row shows the image templates extracted from images of comparable resolution but different illumination conditions after the iterations in step 4 and 5 have been performed a few times. The second row shows the same mean brightness model that is rendered at the particular geometry of each image. The image resolution ranges from 1.2 – 1 km/pixel and the map scale is 1.5 km/pixel.

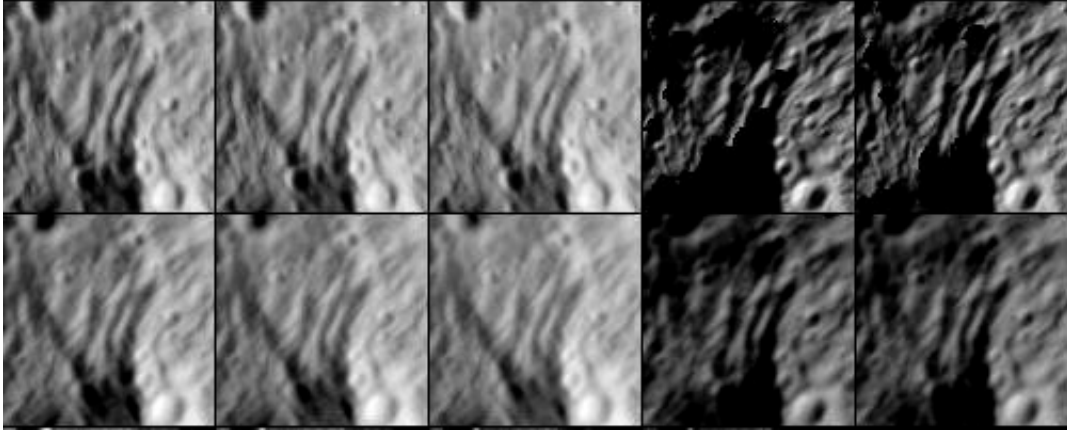


Figure 2. Upper row; image templates from late approach resampled, aligned and projected on the surface. Lower row; the brightness model re-illuminated at the geometry of the respective image

6) The slopes are integrated into local heights. This process requires boundary conditions, which are initial seed heights. These are stochastically sampled from an existing shape model or nearby overlapping maps. The heights are then computed via a relaxation process over many iterations until we have reached convergence.

7) After the map is completed the final step in determining a single landmark map is to search for additional constraints that are used in the global estimation solutions; limb points and map overlaps. If a map can be identified in the limb of an image, the limb condition is an additional constraint of the camera pointing solution in the direction perpendicular to that limb. By design there are always nearby overlapping maps, which share common topography with the current map. Due to projection and illumination effects and because nearby maps may not include exactly the same images, the heights of such overlapping maps may differ initially. Cross-correlation in the overlap area provides a relative vector between these landmarks which may differ from the landmark difference as determined from the construction of these maps. This relative vector is an additional constraint in the global landmark solution.

8) Systematic tiling of the visible surface area. The above steps are repeated until all area that is imaged is mapped, based on the geometric constraints of step 2 above. In the first stages of such tiling, we use latitude, longitude coordinates at a spacing that corresponds to a specific spacing of the landmark maps so that for a given map there is a minimum of 3-4 overlapping maps. Typical spacing is such that there's a minimum of 20% of common surface area shared by nearby maps, and in the first stages as much as 50%.

9) Global solutions: After tiling the surface the next step is to solve for the landmark vectors, camera pointing and camera position via a global weighted least squares estimation that minimizes the difference between predicted and observed landmark pixel, line positions. Initial weights reflect the expected accuracy of the S/C-Vesta position, camera pointing and landmark position based on the accuracy knowledge of the *a-priori* shape where they are projected. The process is iteratively, first solving for the landmark vectors, then for the camera pointing and S/C-Vesta position. At each stage of the iteration the updated covariances are used as inputs in

the next stage. Usually 3 iterations are sufficient for convergence. The estimation of the S/C-Vesta relative position is really a kinematic one on a per-image basis, neglecting all the dynamical data, with some image-to-image constraints based on the predicted velocity uncertainty, so as to avoid a truly random correction among adjacent images. However it is important that the S/C-Vesta vector be included in the estimation process since position correction to some degree correlates with pointing. A common practice has been to always use a realistic predicted position uncertainty from the orbit determination team so as not to over-correct for the relative position. Subsequently the post-fit residuals of landmarks in images and between overlapping maps and the landmark diagonal elements of the position covariance are inspected for outliers. Such outliers could be due to poor correlation of image templates from map projection effects, or due to a particularly dark patch of an image, or very rarely due to mis-identification of features in the cross-correlator. These outliers are usually corrected by hand.

Once we have reached this state the newly created landmarks can be used in the orbit determination process. The inputs to the orbit determination are the body-fixed landmark Cartesian vectors, the diagonal elements of the 3x3 landmark position covariance, the pixel, line location of all landmarks in all images of interest and the pixel, line landmark centerfinding uncertainties.

For a given landmark and image set the above steps are the first stage in a multi-iteration process. Because the map slopes and photometric model is tied to the imaging geometry and the landmark position any improvements in these as a result of the global solutions will improve the model of each map which in turn will lead to more accurate landmark locations. The steps 4 – 9 outlined above are then repeated a number of times, mostly in batch mode using preset processing scripts, until there's no longer reduction of the post-fit residuals. Each of these iterations results in an improved set of OpNav inputs to the orbit determination process.

10) Finally when there is sufficient surface coverage by maps the individual maps are integrated into a shape model. The construction of updated shape models early on in the landmark development process is important in order to correctly project future images on the surface. Accurate image projection results in more accurate estimation of local slopes and albedos and eventually more accurate maps and landmark vectors. Due to operational constraints in accessing the elements of the shape model, our current models are limited to  $\sim 1.56 \times 10^6$  vectors which for Vesta corresponds to a surface separation between adjacent shape model vectors of  $\sim 700$  m. Therefore, the usefulness of the shape model decreases as the image resolution and the map resolution increase which in this mission happens at the end of Survey. After that phase, we synthesize larger format regional maps, up to  $1024 \times 1024$ , which we call "bigmaps", that we use to project images for the construction of a new, higher resolution, set of landmarks. Figure 3 shows an equatorial view of the shape model at the end of HAMO-2.

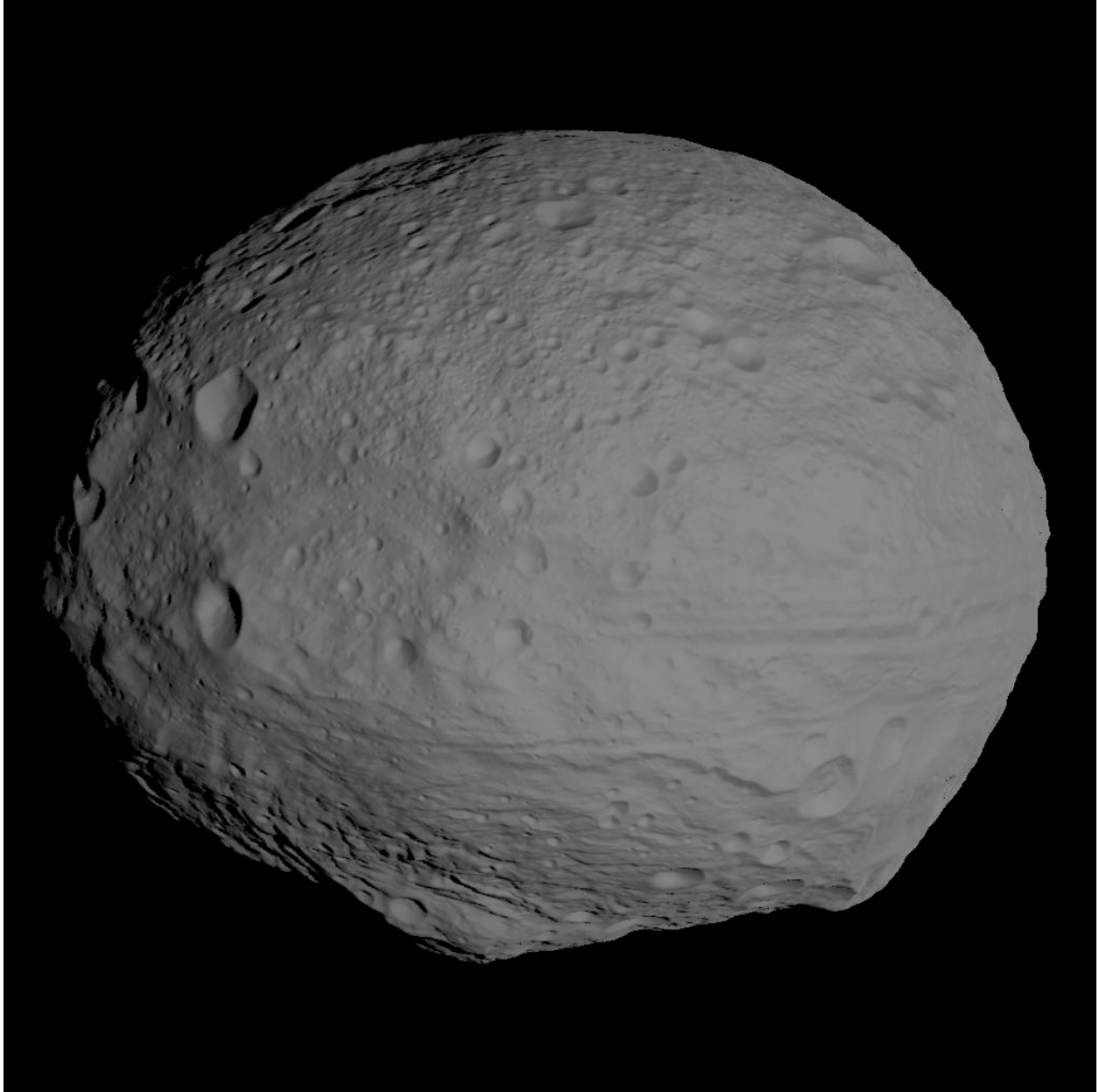


Figure 3. An equatorial view of the shape model of Vesta after the end of HAMO-2. The complex topography of the south pole basin as well as the equatorial troughs is apparent.

## **5. OpNav data acquisition summary**

The OpNav acquisition plan was developed in the 3 years preceding Vesta operations. The plan was evolved iteratively following navigation performance analyses, mission requirements and also taking into account the overall science data acquisition plan. The year preceding Vesta operations, the OpNav imaging plan was merged with that of science on a mission phase basis, into integrated sequence builds that included all instrument and ACS commands as well as all the playback and background sequence commands. These sequences received only minor changes

during Vesta operations, mostly in exposure durations and in the absolute epoch that defined the beginning of each sequence.

The pre-Vesta established plan for image acquisition was carried out almost as planned with the exception of a few instances were anomalies, such as S/C safing events or instrument issues prevented either the acquisition or the playback of the images.

**5.1 Approach:** A total of 24 OpNav sessions were scheduled out of which 23 were executed. These varied in duration and frequency from ½ hour every week in early approach to 1-2 hour long every few days in late approach. They include the 4 RCs that last a full Vesta rotation period, 5 h 20 min. When Vesta was predicted to be < 1 FOV, up to OpNav19, these were planned as star-relative observations. Due to the large brightness ratio between Vesta and background stars, which the dynamic range of the detector could not accommodate, the star-Vesta observations alternated between long star exposures and short Vesta exposures. The 5 OpNav opportunities during late approach and spiral to Survey were placed so as to acquire to the extend possible a complete surface coverage at varying views for constructing landmarks.

**5.2 Survey:** There were a total of 6 dedicated OpNav sessions, 1 per orbit, of 2-hour duration following the dark-to-lit terminator crossing, offering complete longitude coverage of north latitudes in the 50° N - 20° N range. Two mosaics, one equatorial and one polar, in a 1x3 offset pattern over a full rotation period. These mosaics were deemed sufficiently important so that for redundancy reasons they were repeated. The mosaics covered all longitudes, but with some gaps, between 25° N - 90° S. Science imaging, pointing at fixed offset relative to Vesta over a full rotation period at various orbits filled any existing gaps and offered an additional rich dataset. A total of 854 clear filter images were acquired.

**5.3 HAMO-1 & HAMO-2:** There were no dedicated OpNav images. Instead all of the science clear filter images acquired for topography were used for navigation as well. Two of the off-nadir cycles had pointing optimized for SPC with emission angles in the ~40° - 45° range and the other two were optimized for stereo-photogrammetric topography methods. On the average ~2500 clear filter images were acquired for each of these phases, the only loss being a complete orbit in Cycle 1 of HAMO-1 due to a camera anomaly.

**5.4 LAMO:** As with HAMO-1 and HAMO-2, there was no dedicated OpNav imaging, but all clear filter images were used. During LAMO Dawn was pointed to Vesta center and consequently all images were either nadir or at a very small off-nadir angle, due to small trajectory and pointing errors. The LAMO acquisition plan was designed in cycles that lasted 4 weeks each. Each cycle had a different pattern and volume of images acquired in order to accommodate the playback of the other instruments and/or the acquisition of color images. The total number of images per week varied from as few as 120 in Cycle 3 (February 2013) to as many as 630 in Cycle 5 (April 2013).

**5.5 Transfers:** Few OpNav sessions were planned for the Survey-to-HAMO-1 and HAMO-1-to-LAMO transfers. Transfers were dedicated to continuous thrusting with a few interruptions for acquiring tracking data and images. A particular difficulty for planning OpNavs during the transfers was the fact that the S/C flight path control was phase-free relative to Vesta, making planning in advance for certain time windows within which to acquire images very risky that the

images could be acquired on the dark side of Vesta. For the transfer to HAMO-1 we had planned 3 OpNav opportunities, but for each of these we had sequenced 3 different possible times spaced roughly  $120^\circ$  around Vesta from which we selected to execute one, once the actual Vesta phase was known. For the transfer to LAMO no such planning was possible and from the 7 total OpNav sessions  $\sim 3/4$  of the data were on the dark side of Vesta and unusable.

## 6. Approach Operations

The main objectives of the OpNav effort on approach was to assist in the orbit determination and orbit insertion in Survey. Part of that effort was estimating the first important Vesta parameter, its rotation axis, which began when the first set of landmarks were constructed.

Overall image acquisition and processing was executed as planned, with one anomaly only, a safing event that prevented the acquisition of OpNav14.

There were 40 full frames per session alternating between short exposures for Vesta, in the 9-7 ms range, corresponding to a phase angle  $42^\circ - 30^\circ$ , and the longer star exposures of 1.5 s, that were required to image 8<sup>th</sup> - 9<sup>th</sup> visual magnitude stars. The long exposures overexposed Vesta by a factor of 30 above full well. Fortunately, the out of field scattered light was significant only close to Vesta so that most stars were unaffected in early approach. Analysis showed that the scattered light was equivalent to a 7th mag. star at an altitude  $\sim 1000$  km from Vesta, which meant that we could not image stars from OpNav18 and later when Vesta reached 500 pixels across. Figure 4 shows a long exposure from OpNav2 with stars down to 9<sup>th</sup> mag. and the saturated disk of Vesta. Figure 5 shows a 9 ms exposure image from the same session with Vesta and the superimposed projected disk of a triaxial ellipsoid, taken at  $\sim 10^6$  km range. Vesta is 6 pixels across at a resolution of  $\sim 87$  km/pixel.

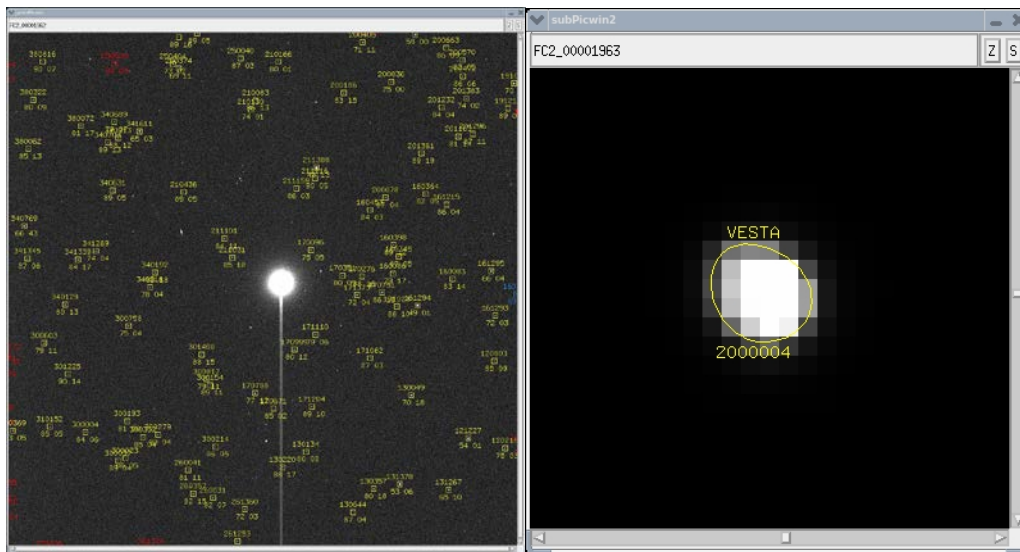


Figure 4 (left). Full frame of a 1.5 s exposure image from approach observations of saturated Vesta at the center and the star background.

Figure 5 (right). Close-up of a 9 ms exposure image, showing Vesta with a superimposed ellipsoid disk.

The inertial camera pointing was estimated from the stars, with post-fit residuals of 0.08 – 0.11 pixels. That camera pointing solution was propagated from the time of the long exposures to the time of the short exposures in order to estimate the inertial pointing of these images. The pointing interpolation was performed with an exponentially decreasing time correlation between the Vesta and star images, with a time constant roughly twice the image separation. The method uses the pointing correction from the star images and the nominal ACS pointing from all images in order to interpolate the pointing correction of the Vesta images. In Figure 6 we show such an example of interpolated pointing values from OpNav2

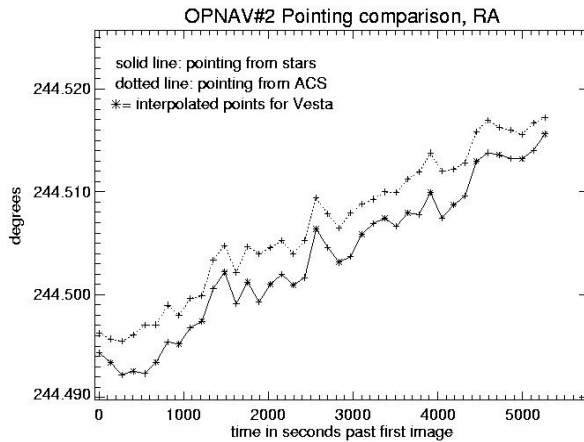


Figure 6. The interpolated Right Ascension values for the pointing correction at the Vesta image times interpolated from the correction at the times of the star images.

Based on the inertial pointing errors and the noise in the ACS data the accuracy of this method was estimated to be  $\sim 0.2$  pixels ( $1-\sigma$ ). On two instances where we serendipitously had two, 2<sup>nd</sup> & 3<sup>rd</sup> mag. stars in the Vesta images, and therefore were able to establish the camera pointing independently we could confirm that the accuracy of this method was indeed at least 0.2 pixels. An inertial pointing comparison between star images, which was regarded as the “truth”, and ACS was conducted with the 16 OpNav sessions that imaged stars, to establish the expected ACS pointing errors for the other mission phases, which was measured to be 0.9 pixels ( $1-\sigma$ ). For the first 11 OpNavs, where Vesta ranged from 5 – 40 pixels across we used only limb scans to estimate the CoF. As expected the number of converged scans perpendicular to the limb increased with the size of the body from 6-8 scans/image in Opnav1 to  $> 100$  scans/image in OpNav16. Similarly the centerfinding Vesta uncertainty decreased from 0.5 pixels in OpNav1 until it flattened to  $\sim 0.15$  pixels in OpNav8 and later. There were two choices for the *a-priori* shape model that we used in the limb scan fitting. One was a triaxial ellipsoid, based on the best-fit triaxial model from the HST observations [19] with semi-major axes,  $a=289$  km,  $b=280$  km and  $c=229$  km and the other was the shape model extracted from these observations, which even though very coarse it modeled the outline of the south pole crater far better than the ellipsoid [19]. One surprising result, was that the triaxial ellipsoid worked better with the limb scans compared to the shape model. Overall, the number of images for which there was no convergence in the CoF estimation with the shape model was quite high,  $\sim 25\%$ , and the scatter of the centerfinding results larger as compared to the triaxial ellipsoid. One tentative explanation is that the representation of the shape model in terms of spherical harmonics was not sufficient to capture the details of the surface irregularity as projected in the image which resulted in fewer limb scans converging. This topic is still under investigation.

Starting with Opnav12 (or RC1) the first set of landmarks was constructed. A total of 36 Vesta images were acquired spaced  $10^\circ$  in Vesta rotation. This particular session was chosen following analysis that included high-fidelity simulations to establish the earliest time that landmarks could be constructed. At that range,  $\sim 10^5$  km, Vesta has an apparent diameter of 62 FC pixels, with 9.3 km/pixel. The challenge is to construct landmarks with maps small enough relative to the curvature of the surface. A number of combinations of map grid sizes and resolutions were studied and we finally decided on 99x99 maps at 1.5 km/pixel. Maps with fewer grid points, say 25x25, and map scale closer to the image resolution did not cross-correlate as well due to the smaller number of map pixels. Constructing maps at a scale 6x higher than the image resolution is at the limit of the applicability of the method and the map intrinsic resolution is really closer to 10 km rather than that of the map scale. However, by adding higher resolution images at later times to the same landmarks, eventually the average image/map scale is reduced. With the sub-S/C Vesta latitude at  $-33^\circ$ , the surface image coverage is limited to the southern hemisphere and up to  $10^\circ$  N. We tiled the surface systematically starting at  $5^\circ$  N, moving at steps of  $12^\circ$  in longitude and  $10^\circ$  in latitude near the equator, and gradually increasing the longitude spacing to  $45^\circ$  at  $75^\circ$  S, for a total of 211 landmarks. Depending on the lat/lon of Vesta each landmark contained between 4 - 20 images with fewer images in the equator and more images at the south pole.

After their initial construction these landmarks underwent many of the iterations outlined in the previous section in order to reduce the residuals of the global fit between landmarks & images. After the first iteration the RMS of residuals between images and landmarks as well as between overlapping landmarks, was 3.9 km (or 0.43 image pixels) and the RSS of the diagonal elements of the landmark covariance averaged over all landmarks, 2.0 km. The latter is a measure of the landmark height error. At the end of each of these iterations a delivery was made to orbit determination. Figure 7 shows the extracted and modeled image brightness for a particular landmark map. As expected there's an apparent lack of feature definition given the large image/map scale ratio. Finally the first shape model was constructed from these maps, covering mostly the southern hemisphere. Figure 8 shows an equatorial view of that model. Although quite coarse with a true resolution of no better than 10 km, re-projection of the same images on this shape model further reduces the post-fit residuals to an RMS of 2.7 km or 0.29 FC pixels and the average of the RSS landmark covariance to 1.5 km. The total number of observations, defined as the sum of all pixel, line pair of landmark observations in all images is 5124.

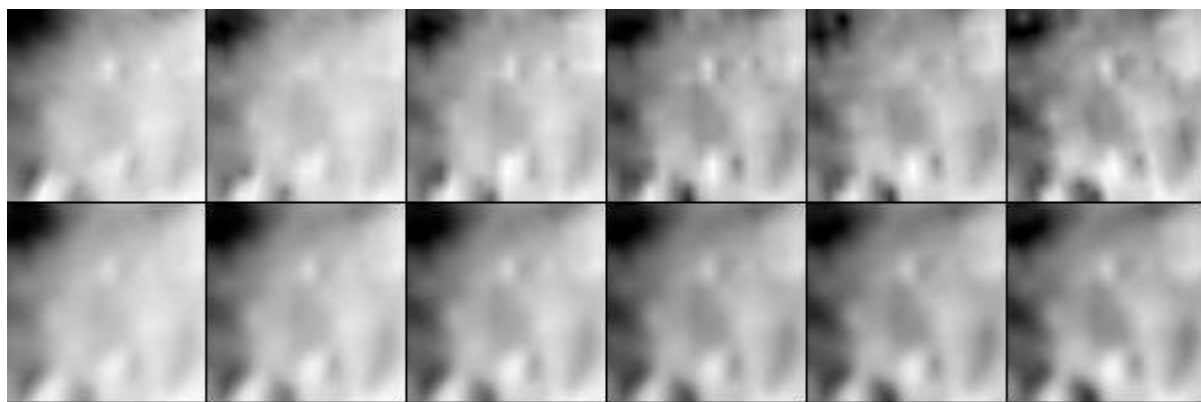


Figure 7. A section of the extracted and modeled brightness map model at 1.5 km/pixel from RC1 images at 9.3 km/pixel. Even though there's poor feature definition, the brightness contrast is sufficient to allow accurate sub-pixel correlation between images and map.

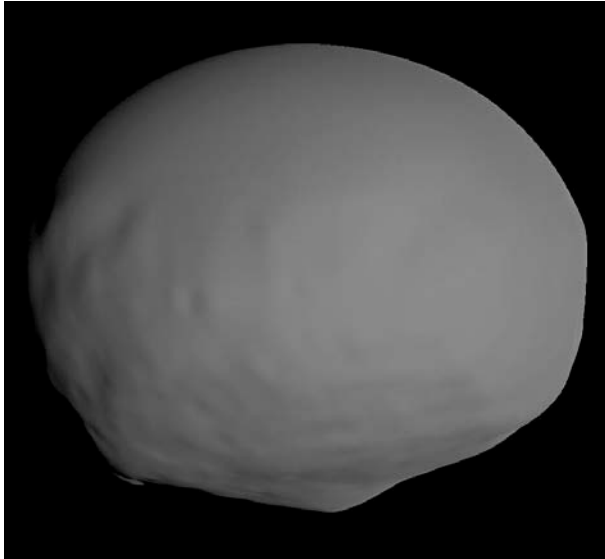


Figure 8. The first shape model on approach to Vesta from the RC1 observations. The area south of  $10^{\circ}$  N is the rough topography from the RC1 images, whereas the area north of  $10^{\circ}$  N is the original featureless shape model from HST observations. Even though very coarse, it already shows the outline of the south regions topography

During the next five data sets OpNav13, RC2, OpNav16-18, the S/C moved to progressively further southerly latitudes with the last two sessions crossing the south pole, while reducing the range to Vesta to 10800 km. Consequently the surface coverage remained the same and there was no need for adding any new landmarks. Instead the new images were added to the existing landmarks as follows;

- a) all current landmarks within certain geometric were added in each new set of images. A pointing solution was performed based on the landmark location and the initial trajectory and image pointing. This process allows a quick input to orbit determination without modifying the landmark vectors
- b) landmarks that are included in the new images are rebuilt, with new slopes and heights estimated. A global fit is performed that solves for the pointing and landmarks based on all images. This process, time permitting, may iterate a few times, each time checking for outliers. At the end of this process another delivery to the orbit determination is made, with, in principle, modified landmark vectors. The pixel, line landmark location of past images can change as a result of adding new images to the same landmark, and therefore the whole set of past observations has to be re-delivered in this process. If needed, an improved trajectory based on both the optical and radiometric data may be used to update the nominal S/C position prior to the landmark re-estimation.
- c) As needed a new shape model is constructed. Due to the rapid change in image resolution, from 9.3 km in RC1 to 0.9 km in OpNav18, an updated shape model was constructed after each new image set was processed.

Most of the images were added to the south-latitude landmarks and at the end of this phase the number of landmarks per image in the south had increased considerably; up to 60 images/landmark at the end of RC2 and up to 110 images/landmark at the end of OpNav18. The inclusion of a large number of images, many of which are at very similar geometry and illumination is not really necessary for improving the topography maps, but it is beneficial to the orbit determination process, and for that reason all images were retained. At the end of RC2 processing, the average of the RSS landmark covariance was reduced to 1.07 km, the post-fit residuals RMS to 1.66 km for a total of 10844 landmark observations. At the end of OpNav18 processing the average RSS landmark covariance was 0.7 km and post-fit RMS residuals to 1.3 km for a total of 15671 landmark observations. Figure 9 shows close-ups of Vesta images from some of the above sessions.

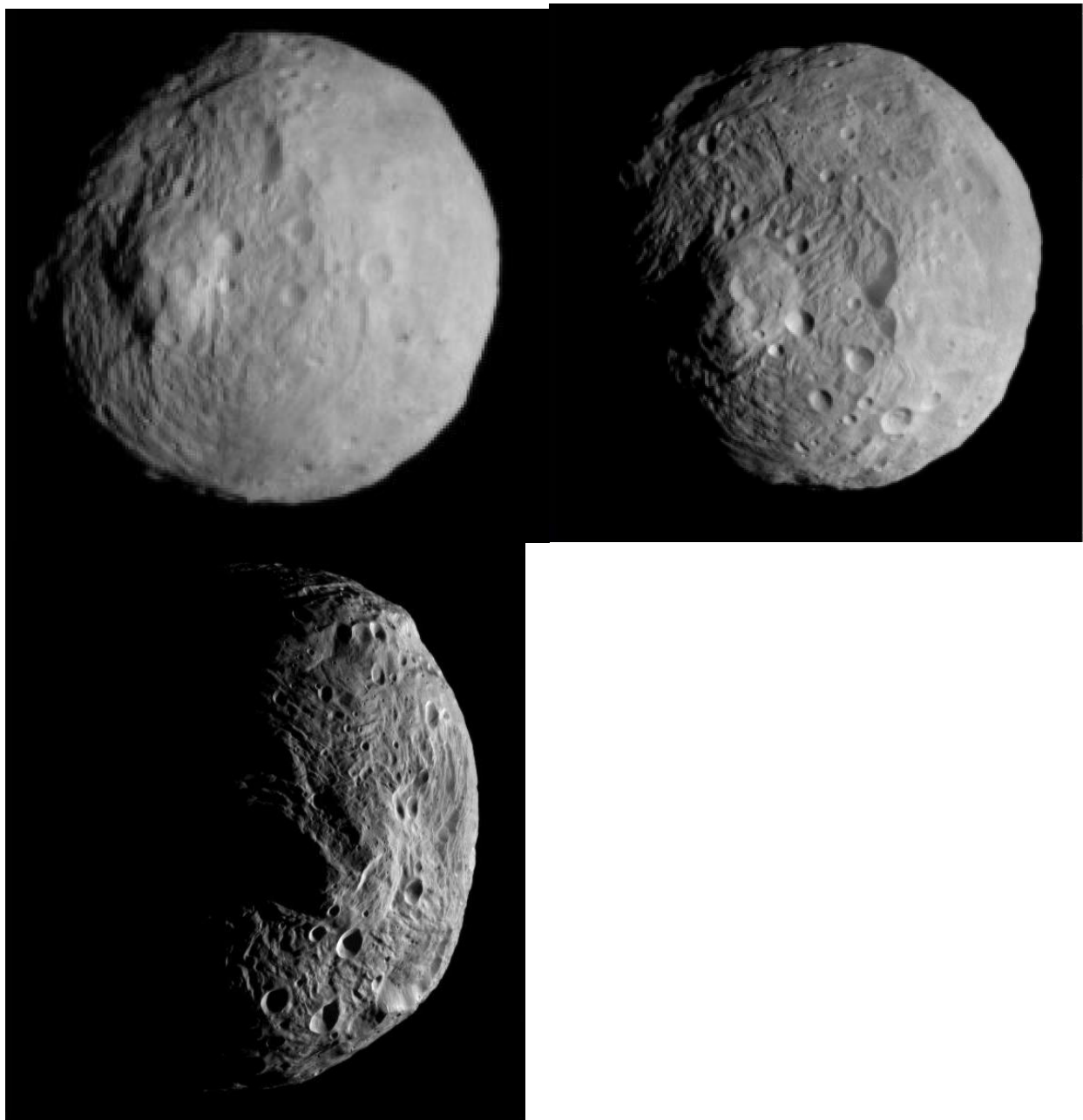


Figure 9; images from RC2, (upper left), from Opnav16 (upper right) and from OpNav18 (lower left) showing Vesta as seen from approach. The complex topography of the southern pole basin and its central peak is clearly visible.

The next set of images on approach are acquired while Dawn was completing its first revolution about Vesta, on the daylight north to south pass and are Opnav19, a 3-hour imaging of mid north latitudes, RC3 centered at equator crossing, RC3b, the backup to RC3 centered at latitude  $27^{\circ}$  S, where the phase angle was at its minimum of  $12^{\circ}$ , to allow the best radiometric calibration of VIR, and OpNav21 looking nadir towards the south pole. The combination of these observations aim to provide almost complete surface stereo coverage from  $40^{\circ}$  to the south pole at 500 m/pixel, including the first ever view of the northern hemisphere. Aside their immediate use in navigation, these data were also used to estimate the pole of Vesta for the reference trajectory design for the Survey to HAMO-1 transfer and for HAMO-1 insertion. In addition these data were used to construct the landmarks for early OpNav processing in Survey.

Prior to begin processing these images we thinned out the earlier ones, so that every other image from RC2, and Opnav16-18 was discarded, in order to keep the number of images per landmark manageable. This theme of dropping early images was repeated a couple of times up to the end of Survey, especially when creating higher resolution landmarks. This data set was processed following the above outlined steps. Subsequently we tiled the newly exposed northern hemisphere of Vesta in the same lat,lon stepping scheme,  $10^{\circ}$  in latitude and  $12^{\circ}$  N-  $15^{\circ}$  N in longitude, with landmarks centered up to  $35^{\circ}$  N, which exhausted the north coverage, for a total of 295 landmarks. Next all RC1 and OpNav13 images were removed, since they were a factor of 20 coarser resolution than the recently acquired images which offer the same surface coverage and the steps described in part (b) above were performed a few times.

The next step was constructing landmarks to use for early OpNav processing in Survey. To that end the imaged surface of Vesta was tiled again with landmark maps, at resolution 750 m/pix, or a factor of 2.5 coarser than the average Survey image resolution. A total of 520 maps at 750 m were constructed every  $10^{\circ}$  in latitude and with longitude spacing that varied from  $10^{\circ}$  at the equator to  $20^{\circ}$  at the south pole. The spacing was such as to ensure a minimum of 35% surface overlap between adjacent maps. The endpoint of approach was a total of 816 landmarks at 1.5, 1 and 0.75 km resolution, with a post-fit RMS residuals of 554 m and an average RSS position covariance of 225 m. There were a total of 61602 landmark observations with 255 images contributing. Figure 10 displays some images from the late approach observations.

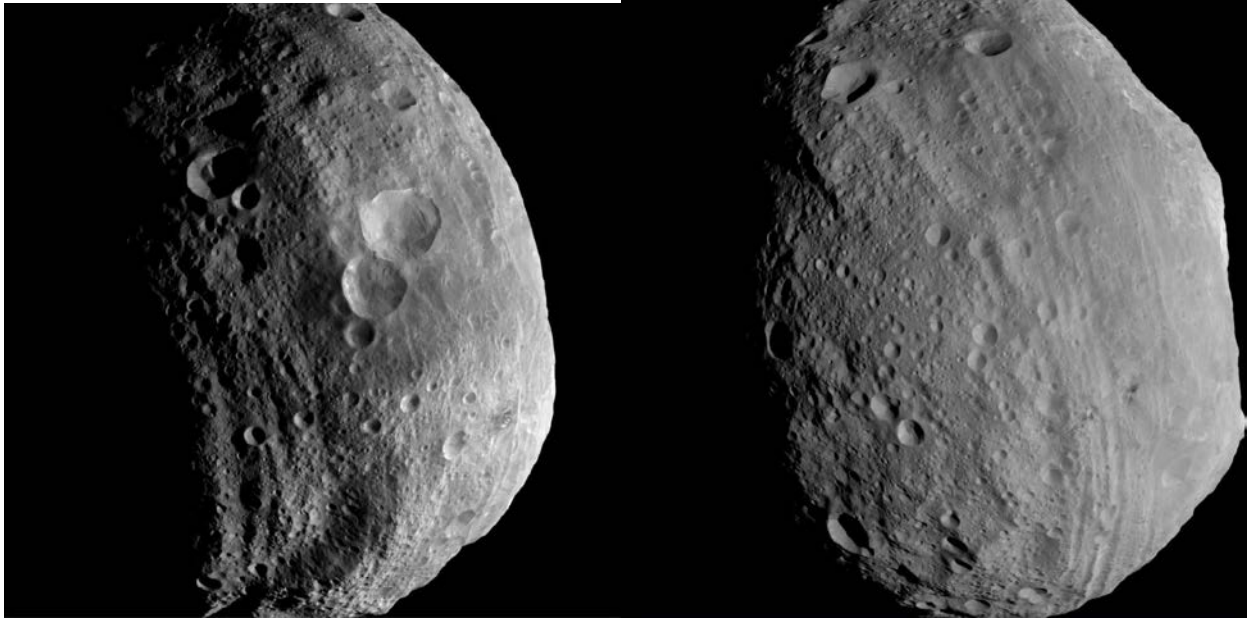


Figure 10: Left, an image from OpNav19 showing some of the northern hemisphere terrain, including the “snowman” triple-crater feature. Right, an image from RC3 showing the equatorial troughs and the south pole outline.

## 7. Pole estimation from approach observations

The first important Vesta parameter that had to be estimated beginning with the approach data was the Vesta pole. The initial values were set from the Dawn Science team after careful analysis of the ground and HST data sets to be  $RA=305.8^\circ$ ,  $DEC=41.4^\circ$  [20].

An improved estimation of the pole was needed for the final trajectory design for insertion into all science orbits including the transfer to these orbits. The time needed by mission design to build these trajectories required that the pole updates be available at some earlier time; for Survey orbit insertion 2 days after Opnav18 and for the transfer from Survey to HAMO-1, 5 days after the RC3 data acquisition. In principle the pole can be estimated by both optical data (landmarks) and radiometric data (Doppler). In practice both data sets were used, however on approach the main data were landmarks. From simulation and covariance studies we expected that beginning with RC1 we could begin updates to the pole with an expected error of  $\sim 0.4^\circ$  ( $1-\sigma$ ) and that the RC3 block of observations would significantly improve the accuracy to the level of  $0.03^\circ$  ( $1-\sigma$ ). In figure 11 we show a summary of a few of our converged OpNav solutions at the end of processing of a particular data set. As “truth” for comparison we take one of our solutions with the combined data set from LAMO, which is significantly more accurate than what we could accomplish on approach. The first obvious conclusion after processing the RC1 data was that there was a significant correction, by more than  $3^\circ$  in the initial value of the right ascension. The pole solution from RC1 is already within  $0.2^\circ$  from the truth, however later updates, RC2 and OpNav18 tend to deviate further away. This, despite the fact that in later updates all the earlier data from RC1 are included in the solution. Finally, as expected the RC3 data move the pole solution within  $0.04^\circ$  from the truth. These results are surprising and currently under investigation as lessons learned for Ceres. The most favorable explanation is that the results are due to the observing geometry; beginning with RC1, which is at mid-south

latitudes, subsequent observations image Vesta further south and up to the south pole. These observations, even though at higher resolution do not seem to have as much strength in the pole estimation as observations closer to the equator as those from RC1 and RC3.

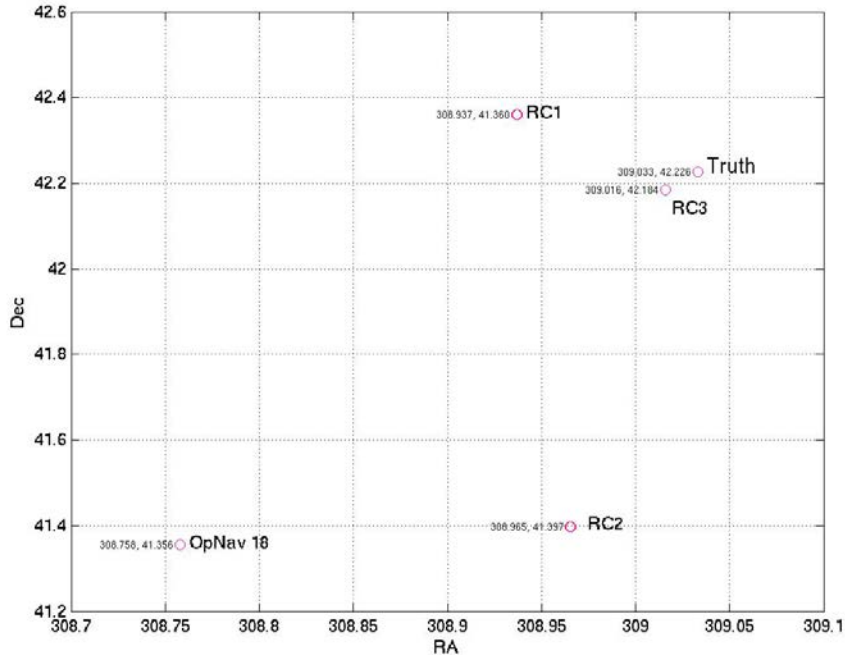


Figure 11. A few of the OpNav pole solutions on approach. Shown are the final converged values at the end of processing of the respective data set.

## 8. Survey Operations

Prior to beginning Survey operations we discarded all images less than 500 m resolution, which resulted in a relatively short data arc, extending over a two-week period only. For each of the seven orbits downlink of images began 2 hours after the lit-to-dark terminator crossing. Standard processing with every new data batch began by executing steps a and b as described above for approach. The surface coverage of the available data set was also estimated. Subsequently, if there was time available before the arrival of new images, areas where there was sufficient coverage with Survey images, typically 5 or more, were tiled with the next round of higher resolution landmarks, which was at 300 m/pixel, the nominal Survey image resolution. As early as the end of the first Survey orbit, there was sufficient equatorial and polar coverage to begin the tiling in these areas. Tiling proceeded by dividing the surface area up to 60° N with 41 overlapping larger size maps, 256x256, at 750 m/pixel, which were constructed prior to Survey. This process was executed entirely in batch mode, running scripts that would follow all steps in the construction of a new landmark. The new landmarks were defined at specific coordinates relative to the bigmaps with a stepping scheme that allowed ~40% surface overlap between neighboring maps. The only manual work required in the processing of these new landmarks was checking and correcting for outliers. By the end of the 3<sup>rd</sup> orbit we had achieved complete surface coverage and by the 4th orbit all 300 m maps required to cover completely the visible surface of Vesta, a total of 2300, have been created. The procedure of round-the-clock

processing of new images and the continuous rebuilt of landmarks was interrupted at predetermined intervals in order to provide inputs for the orbit determination, of which a total of 10 were made in Survey. At the end of Survey, we removed all remaining approach images from the landmarks, discarded the landmarks that were at resolutions of 1.5 and 1 km, which were too coarse to be of future use, and rebuilt all landmarks one more time for a preliminary Survey orbit reconstruction. At this point the average value of the RSS of the landmark covariance was 97 m, for a total of 209528 landmark observations and the post-fit RMS of residuals was 88 m, or 0.29 Survey image pixels. This last figure includes the contribution to the residuals from map-to-map overlaps and the limb-landmark constraints. The RMS of residuals between image and landmarks is even smaller at 0.15 FC pixels.

However, the landmark height error distribution was not uniform. Image coverage and illumination conditions created systematic errors with regional variations. The landmarks with the highest accuracy, evidenced in both the post-fit residuals and individual landmark covariance were in the  $50^{\circ}$  S to  $90^{\circ}$  S latitudes. The reason was not only the larger number of images per landmark but also the fact that these regions enjoyed almost complete azimuthal coverage in solar incidence and variation in solar elevation. The landmarks with the larger position errors were concentrated in two places. The first was landmarks along the northernmost narrow band. Many of these landmarks had relatively dark images, at very low solar elevation,  $< 10^{\circ}$ , some of them contained large, dark patches due to topography and they had no landmark neighbors to their north. The second was a band of  $\sim 30^{\circ}$  width in latitude centered at  $27^{\circ}$  S where the phase angle was the minimum of  $12^{\circ}$ - $15^{\circ}$  throughout Survey. These landmarks suffered from high solar elevation, with small azimuthal variation. The effect of the high solar elevation was to wash out fine topographic information resulting in maps that contained mostly albedo information with inferior slope estimation. This problem, which was also apparent in the RC3b images on approach, was already known from high-fidelity simulation studies and it is inherent in the orbit design choice of a small beta angle. To counter this undesirable effect the OpNav inputs included alternate deliveries where the landmarks in the low-phase sub-equatorial band were excluded.

The final step in Survey was to construct the landmarks needed for HAMO-1 and the other mission phases. HAMO images are at a nominal resolution of 60 m/pixel, a factor of 5 higher than that of the 300 m map resolution, which would have resulted in sparse landmark coverage of the HAMO images. From past analysis a factor of 2-3 in map/image ratio was needed in order to provide good landmark image coverage and adequate correlation between maps and images. The process that we used to construct the 300 m maps, was repeated during the  $\sim 3$  week long transfer from Survey to HAMO-1. The surface of Vesta up to  $60^{\circ}$  N was divided into 49 regions of overlapping large size maps,  $512 \times 512$  at 300 m resolution, which were synthesized from the individual landmark maps. These maps were tiled systematically with higher resolution landmarks, 125 m/pixel. A total of 14828 such landmarks were constructed. We need to emphasize that maps at scale smaller than the image pixel scale do not have a higher intrinsic map resolution. The actual feature resolution in these maps does not exceed the image resolution. Because of the large computational task this work was carried out in a distributed environment simultaneously for each region and the new landmarks were collected in a central node where the global solution of landmarks and camera pointing was performed. The iterated results had a post-fit RMS of residuals of 62 m and an average landmark position uncertainty of 65 m, for a total of  $> 1.2 \times 10^6$  observations and were used in the final Survey reconstruction. Figure 12 shows the

post-fit landmark residuals in both pixel, and line in the final iteration of the combined optical and radiometric data set. The RMS is 0.145 pixels, with few outliers > 1 pixel.

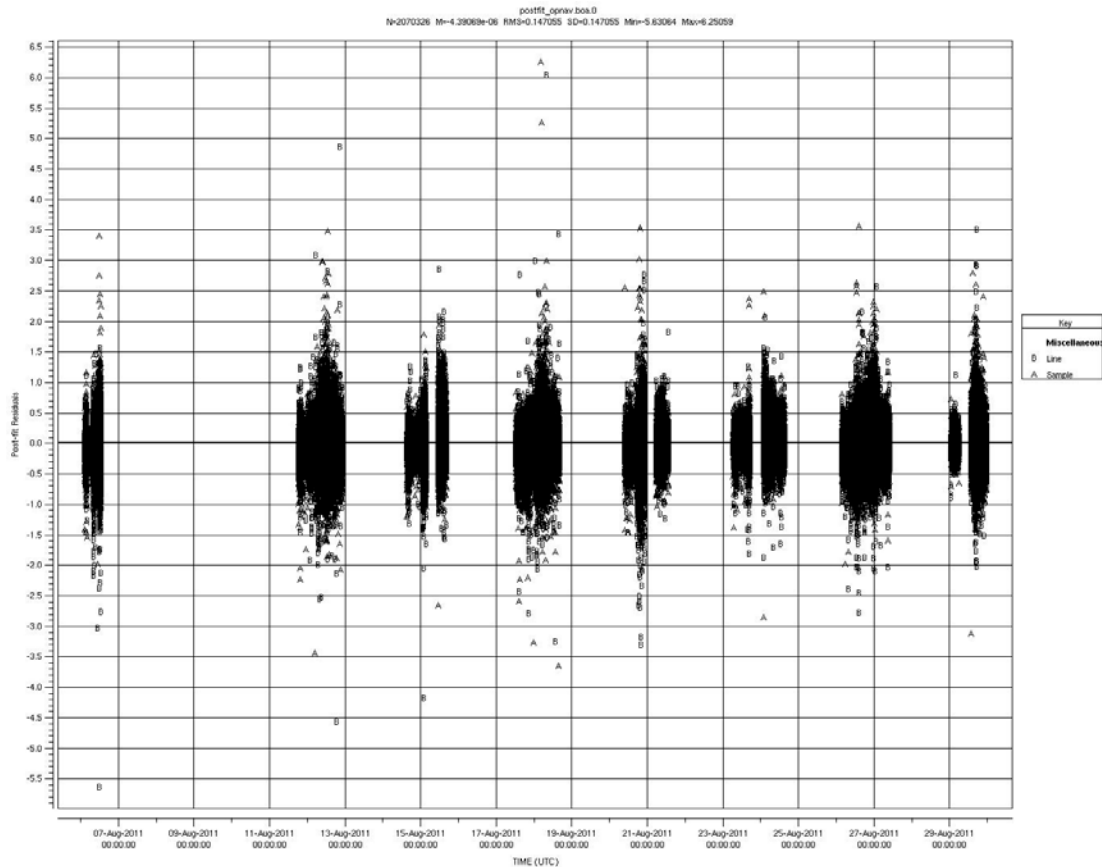


Figure 12. Post-fit optical landmark residuals at the end of Survey.

## 9. HAMO-1 and beyond

The methods and procedures outlined for Survey operations were carried to the other 3 science orbits, HAMO-1, LAMO and HAMO-2, so we'll give a brief summary and only highlight a few interesting points.

### 9.1 HAMO-1

Data acquisition in HAMO-1 was on every daylight 6 hour pass. We had data playbacks roughly every 12 hours. The frequency of the playbacks and the large number of landmarks present allowed little available time in which to rebuild all landmarks with the addition of the new images, while in HAMO-1. Furthermore, each cycle in HAMO-1 covered completely just once the visible surface, so at the end of each cycle, there were no more than 2 new images to contribute to each landmark with the exception of the south pole. After cycle 3 we began rebuilding mostly the sub-equatorial latitude landmarks, which in Survey suffered from the high solar elevation. The addition of the HAMO-1 images at a minimum of 30° phase in that region, significantly improved the surface feature resolution there, the landmark-to-image correlation and eventually the accuracy of the landmark position. Figure 13, shows such an example; there

are many surface features that span lengths from a few to many Survey image pixels, yet many of them appear fuzzy or unresolved at the end of Survey, but they are completely resolved after adding a few HAMO-1 images at lower solar elevations.

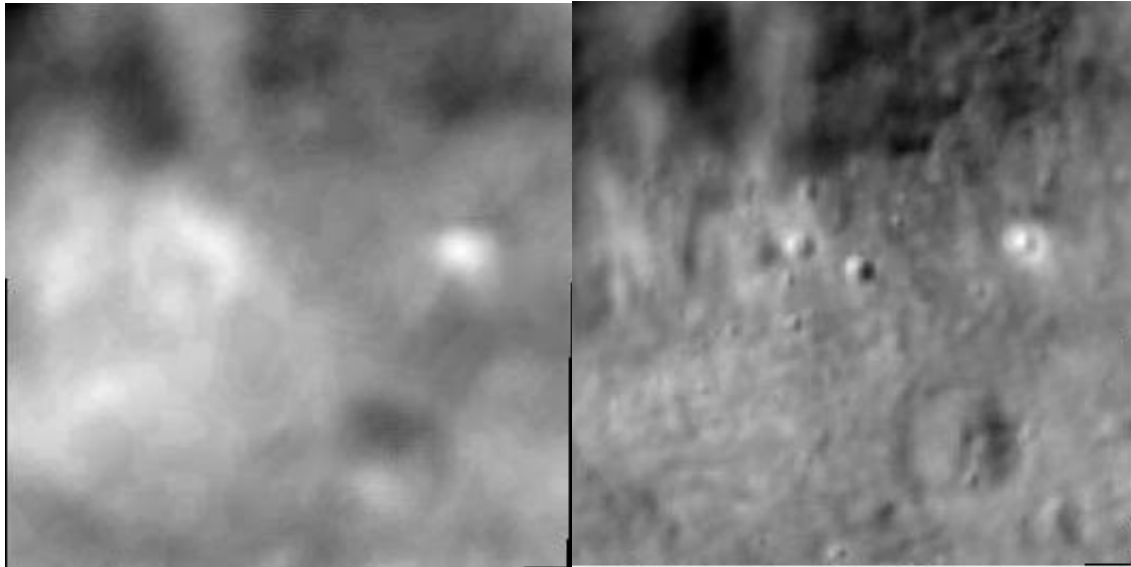


Figure 13. A 125 m/pixel map at 20° S latitude. Left; as it appears at the end of Survey. Right; after we have added a few HAMO-1 images at lower solar elevation

One of the interesting findings early in HAMO-1 was a shift between the center of the coordinate system of the landmarks and the center of mass as established by the radiometric data. Such a drift between the two coordinate systems was potentially expected starting with late approach but no such evidence was found even in Survey. In principle there's no reason why the two coordinate centers should coincide, considering that landmarks are not sensitive to dynamical measurements. In practice we expected that the two coordinate centers should be close given the combined contribution of both radiometric and optical data in the orbit solutions. The telltale sign was a systematic shift between the landmarks, created with Survey data, and the HAMO-1 images. The images appeared to be shifted relative to the landmarks systematically in the latitude direction and the magnitude of the shift was depended on the latitude, with a maximum value of ~700 m near the equator and decreasing to almost zero at the south pole. The exact offset of the two coordinate systems was estimated by the orbit determination team, by solving for the relative vector difference between the two coordinates systems in the process of fitting the radiometric and optical data. This process took place in four iteration steps; at each step the landmarks were shifted by the difference between the two coordinate systems and new inputs were made, until the difference was  $< 6$  m in magnitude. The total shift was 680 m in the +Z direction, i.e. the landmark coordinate system was originally south of the center of mass. The shift in the two equatorial axes was in the order of a few cm only. The most likely explanation for the shift being entirely along the Z axis is that while the radiometric data were influenced by all parts of the Vesta interior, the optical data were limited to covering up to 45° N latitude, so that the number of landmarks were not averaged above and below the equator.

At the end of HAMO-1 the 750 m/pixel landmarks were discarded as too coarse for the remaining mission phases and the remaining landmarks were rebuilt with the addition of the HAMO-1 images. Following that, the visible surface of Vesta was again divided into 85 overlapping regions mapped with large format bigmaps, 1024x1024 at 125 m/pixel and was tiled again systematically with landmarks at 60 m/pixel resolution, the average FC pixel scale of HAMO-1. A total of 52211 landmarks at 60 m/pixels were constructed, bringing the total number of landmarks of 300, 125 and 60 m/pixel to 69242 that were used for image processing in LAMO and HAMO-2. A total of 2533 HAMO-1 images were used. This was the highest resolution of landmark maps created at Vesta. At the end of HAMO-1 the final post-fit RMS of residuals was 28.3 m, or 0.47 HAMO-1 image pixels and the average landmark position uncertainty 44.3 m.

## **9.2 LAMO**

This phase was extended to last ~five months from December 2012 to end of April 2013. Since the key science were GRaND and gravity science the image acquisition strategy and volume was limited by the remaining playback volume. There were 3 playbacks/week that varied greatly in the total number of orbits covered and images acquired from 120/week to 630/week. The image resolution varied with latitude from 22 m/pixel at the south pole to 19 m/pixel at the equator. During the second half of LAMO the Sun had moved sufficiently north in Vesta latitude, up to 12° S, to allow newly exposed terrain in the 50° N - 55° N. However, the larger beta angle in LAMO, 45°, rendered these areas very dark and no new landmarks were constructed there. Usually the first 5-6 images from every orbit were in the north and too dark to be useful. A total of 9045 LAMO images were processed. Because of the very small image footprint LAMO imaging did not completely cover Vesta more than 2 times and most landmarks did not accrue more than 2-5 LAMO images, with the exception of those south of 80° S. Due to the large number of landmarks and images, which rendered processing of the OpNav inputs by the orbit determination team very time consuming, our inputs were limited to a truncated set, usually every second or third image.

The most interesting finding in LAMO was that of a correction to the initial Vesta rotation rate. Shortly after processing LAMO images, it became apparent that there was yet another systematic discrepancy between the surface registration of LAMO images and the landmarks as established at the end of HAMO-1. LAMO images would tend to be offset relative to the landmarks mostly in the longitude direction. That offset was latitude dependent; it was larger at the equator, up to 300 m, and decreased towards the poles. At the south pole the offset was completely random. The obvious explanation was that of a rotation rate error. The Vesta rotation rate until then had been the initial one from ground observations, 1617.3332776 deg/day. Fitting of the radiometric and optical data in LAMO allowed the estimation of a different rate, which at the end of LAMO, with a longer data arc was estimated to be 1617.333125 deg/day.

## **9.3 HAMO-2**

HAMO-2 began with the Sun at 6° S Vesta latitude, so that significant portion of the previously north terrain was now illuminated. HAMO-2 had a similar cycle and observing pattern of nadir and off-nadir observations as HAMO-1 although at a different cadence in order to add more images in the north. HAMO-2 extended the illuminated area of Vesta up to 80° N, but with various dark patches in-between from dark crater interiors. Image processing steps and frequency

were similar to HAMO-1 with the exception of the first 5-6 north images, which initially did not contain any landmarks. At the end of HAMO-2 we began constructing the landmarks in the area between 45° N – 80° N. Because of the absence of any topography there, the sequential landmark construction steps from coarse to finer resolution had to be repeated; first we tiled the area with 300 m/pixel maps and after a first cut shape model that extended to 80° N was completed, the northern latitudes were divided into regions and tiled at 125 m/pixel. Currently we are constructing the 60 m/pixel maps, that we'll use in the final HAMO-2 reconstruction.

## **10. Conclusions**

Overall the OpNav contributions to the navigation operations at Vesta were quite successful. We were able to meet the time-demanding operational constraints, contribute to all phases of navigation and assist in the determination of a number of the physical parameters of Vesta. The first application of landmark navigation for real-time operations produced results at the expected level of accuracy. Key to the successful operations was advance planning of the data acquisition, sequencing as well as simulation and testing of all the steps in the end-to-end navigation processes of the mission. Of equal importance, a number of valuable lessons learned, such as those of the pole estimation on approach, will be followed upon as we begin preparations for the Dawn encounter with Ceres in 2015.

## **11. Acknowledgements**

We are grateful to our colleagues of the Orbit Determination Team, Brian Kennedy, Ryan Park, Sumita Nandi, Rob Haw and Matt Abrahamson and of the Mission Design team, Greg Whiffen, Dan Parcher and John Smith, and to Don Han, the navigation team chief, for the close cooperation, assistance and advice, as well as the Navigation Advisory Group of section 343 for their helpful comments and review of our work throughout Vesta operations. We would also like to thank the members of the Framing Camera operations team and the Sequence Team, both of which were integral in the commanding, acquisition and timely delivery of the images. The work described in this paper was performed at the Jet Propulsion Laboratory, California Institute of Technology, under a contract with the National Aeronautics and Space Administration. Copyright 2012 California Institute of Technology. Government sponsorship acknowledged.

## **12 . References**

- [1] Russell, C.T. and Raymond, C.A. "The Dawn Mission to Vesta and Ceres". Space Sci Rev, Vol. 163, pp. 3-23, 2011.
- [2] Pieters, C.M., McFadden, L.A., Prettyman, T., De Sanctis, M.C., McCord, T.B., Hiroi, T., Klima, R., Li, J-Y., Jaumann, R. "Surface Composition of Vesta: Issues and Integrated Approach". Space Sci Rev, Vol. 163, pp. 117-139, 2011.
- [3] Sierks, H., Keller, H.U., Jaumann, R., Michalik, H., Behnke, T., Budenhagen, F., Büttner, I., Carsenty, U., Christensen, U., Enge, R., Fiethe, B., Gutiérrez-Marqués, Hartwig, H., Krüger, H., Kühne, W., Maue, T., Mottola, S., Nathues, A., Reiche, K.-U., Richards, M.I., Roatsch, T.,

Schröder, S.E., Szemerey, I., Tschentscher, M. “The Dawn Framing Camera”. Space Sci Rev, Vol 163, pp. 263-327, 2011.

[4] De Sanctis, M.C., Corradini, A., Ammanito, E., Filacchione, G., Capria, M.T., Fonte, S., Magno, G., Barbis, A., Bini, A., Dami, M., Fikai-Veltroni, I., Preti, G., VIR Team. “The VIR Spectrometer”. Space Sci Rev, Vol. 163, pp. 329-369, 2011

[5] Prettyman, T.H., Feldman, W.C., McSween Jr., H.Y., Dingler, R.D., Enemark, D.C., Patrick, D.E., Storms, S.A., Hendricks, J.S., Morgenthaler, J.P., Pitman, K.M., Reedy, R.C. “Dawn’s Gamma Ray and Neutron Detector”. Space Sci Rev, Vol 163, pp. 371-459, 2011.

[6] Konopliv, A.S., Asmar, S.W., Bills, F.G., Mastrodemos, N., Park, R.S., Raymond, C.A., Smith, D.E., Zuber, M.T. “The Dawn Gravity Investigation at Vesta and Ceres”. Space Sci Rev, Vol 163, pp. 461-486, 2011.

[7] Raymond, C.A., Jaumann, R., Nathues, A., Sierks, H., Roatsch, T., Preusker, F., Scholten, F., Gaskell, R.W., Jorda, L., Keller, H.-U., Zuber, M.T., Smith, D.E., Mastrodemos, N., Mottola, S. “The Dawn Topography Investigation”. Space Sci Rev, Vol 163, pp. 487-510, 2011.

[8] Brophy, J., “The Dawn Ion Propulsion System”. Space Sci Rev, Vol 163, pp. 251-261, 2011

[9] Thomas, V.C., Makowski, J.M., Brown, M.G., McCarthy, J.F., Bruno, D., Cardoso, J.C., Chiville, W.M., Meyer, T.F., Nelson, K.E., Pavri, B.E., Termohlen, D.A., Violet, M.D., Williams, J.B. “The Dawn Spacecraft”. Space Sci Rev, Vol 163, pp. 175-249, 2011

[10] Whiffen, G.J. “The stability of powered flights around asteroids with applications to Vesta”, AAS Paper 11-186, 21<sup>st</sup> AAS/AIAA Space Flight Mechanics Meeting, New Orleans, Louisiana, 2011

[11] Parcher, D.W., “Thrust orbit transfer design for Dawn operations at Vesta”, AAS Paper, 11-183, AAS/AIAA Space Flight Mechanics Meeting, New Orleans, Louisiana, 2011

[12] Parcher, D.W., and Whiffen G.J., "Dawn Statistical Maneuver Design for Vesta Operations", Paper AAS 2011-180, AIAA/AAS Astrodynamics Specialist Conference, New Orleans, Louisiana, USA, Feb. 13-17, 2011.

[13] Han, D., “Orbit Transfers for Dawn’s Vesta Operations: Navigation and Mission Design Experience”, Proceedings 23<sup>rd</sup> International Symposium on Space Flight Dynamics, Pasadena, CA, USA, 2012

[14] Rayman, M.D., and Mase, R.A. “Dawn’s Exploration of Vesta”, 63<sup>rd</sup> International Astronautical Congress, Paper IAC-12,A3,4,3,x12856, Naples, Italy, 2012

[15] Mastrodemos, M., Rush, N., Vaughan, D., Owen, W., Jr., “Optical Navigation for Dawn at Vesta”, AAS Paper 11-222, AAS/AIAA Space Flight Mechanics Meeting, New Orleans, Louisiana, 2011

[16] Polanskey, C. A., Joy, S.P., Raymond, C.A. “Dawn Science Planning Operations and Archiving”, *Space Sci Rev*, Vol 163, pp. 511-543, 2011

[17] Gaskell R.W. “Digital identification of cartographic control points”. *Photogrammetric Engineering and Remote Sensing* 54(6), Part 1, pp.723-727, 1988

[18] Gaskell, R.W. “Automated landmark identification for spacecraft navigation”. AAS paper 01-422, AAS/AIAA Astrodynamics Specialists Conf., Quebec City, Canada, 2001

[19] Gaskell R.W., Barnuin-Jha O.S., Scheeres D.J., Konopliv A.S., Mukai T., Abe S., Saito J., Ishiguro M., Kubota T., Hashimoto T., Kawaguchi J., Yoshikawa K., Kominato T., Hirata N., Demura H. “Characterizing and navigating small bodies with imaging data”. *Meteoritics & Planetary Science* 43, Nr 6, 1049-1061, 2008

[20] Thomas P.C., Binzel R.P., Gaffey M.J., Zellner B.H., Storrs A.D., Wells E., “Vesta: Spin pole, size and shape from HST images”, *Icarus* 128, pp. 88-94, 1997

[21] Li, J.-Y., Thomas, P.C., Carcich, B., Mutchler, M.J., McFadden, L.A., Russell, C.T., Weinstein-Weiss, S.S., Rayman, M.D., Raymond, C.A., “Improved Measurement of Asteroid (4) Vesta’s Rotational Axis Orientation”. *Icarus*, 211, pp. 528-534, 2011